Experimental evaluation of black liquor carbonation for carbon dioxide capture

(article starts on next page)

Contents lists available at ScienceDirect

Journal of CO2 Utilization
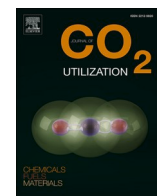
Experimental evaluation of black liquor carbonation for carbon dioxide capture

Emmanouela Leventaki [a],[*], Francisco M. Baena-Moreno [a], Joanna Wojtasz-Mucha [a], Niclas Sjöstedt [a], Abdul Raouf Tajik [b], Gaetano Sardina [b], Henrik Ström [b], Diana Bernin [a],[*]

[a] Department of Chemistry and Chemical Engineering, Chalmers University of Technology, SE-412 96 Gothenburg, Sweden
[b] Department of Mechanics and Maritime Sciences, Chalmers University of Technology, SE-412 96 Gothenburg, Sweden

ABSTRACT

Carbon dioxide is one of the main if not the most potent greenhouse gases responsible for climate change. Scientists put great efforts to tackle this problem and carbon dioxide capture seems to be a promising solution. The present study proposes a novel method of carbon dioxide capture using black liquor, a side stream from the paper and pulp industry. Its content in sodium hydroxide makes it an attractive candidate for carbon dioxide capture via carbonation. The black liquor was prepared from oat husks, a non-woody biomass, using the soda-pulping process. To estimate its carbon dioxide absorption capacity, a mixture of nitrogen and carbon dioxide (70:30%) was sparged into a bubble column reactor and computational fluid dynamics simulations of this setup were used to evaluate the mixing process. The formation of carbonate and bicarbonate ions throughout the carbonation process was followed using a Fourier-Transform Infrared (FTIR) probe and a pH meter. The absorption capacity was measured from the weight increase of the reactor. It was found to be around 30 g of carbon dioxide/L of black liquor. The carbonate and bicarbonate species in black liquor before and after carbonation were further characterized with ^{13}C Nuclear Magnetic Resonance (NMR), X-ray Diffraction (XRD), Scanning Electron Microscope (SEM) and optical microscopy. Using industrial side-streams might enable an economically feasible process without the need for production of virgin absorbents or their recovery. Furthermore, this capturing process, which is performed at atmospheric conditions might reduce the overall energy consumption. The results demonstrated that black liquor could be an attractive absorbent for carbon dioxide, paving the way for a circular and resource-efficient economy.

1. Introduction

Industrially emitted greenhouse gases (GHG) have been polluting the atmosphere and causing severe changes to our climate and quality of life. The effects of GHG emissions are becoming more evident, leading to a worldwide movement towards the establishment of sustainable and greener processes. Many countries have put in place policies to tackle the environmental crisis following the Intergovernmental Panel on Climate Change (IPCC) report, which states the goal for net zero emissions of carbon dioxide by 2050 [1]. To this end, carbon capture has become an attractive option to prevent more carbon dioxide from being released into the atmosphere during our transition from fossil to renewable energy. Carbon dioxide capture might be a temporary solution to collect industrially generated carbon dioxide. The captured gas can then either be deposited in underground reservoirs and stored in a stable mineral form or be reused in industrial applications [2]. Many technologies of carbon capture, utilization and storage (CCUS) have been developed, but unfortunately, large-scale implementation is still limited. The process of carbon dioxide capture needs to be as energy and resource-efficient as possible. If the process has a high energy demand and the energy comes from fossil fuels, the emitted carbon dioxide might exceed the amount that is captured [3,4].

Recently, interest has risen in the use of alkaline industrial waste for carbon capture [5–8]. Utilization of wastes and side streams avoids the production of new virgin feedstock, reduces the energy footprint, and enables valorization—a very important concept of a circular economy. Various industrial residues can be employed for this purpose, and there are already some studies that investigated carbonation methodologies and capture capacity of wastes, such as steelmaking slag [9], construction debris [10,11] and paper mill waste [12–14].

Pulp and paper mills make up an important part of the global industry, which is expected to be growing in the following years. This growth stems from the increasing interest in the use of lignocellulosic biomass to produce various materials as an alternative solution to fossil-based plastics [15]. Trees, the feedstock of this industry, store carbon dioxide, and utilization of the side streams for carbon capture could potentially lead to negative emissions.

In the fiber line process (from the wood feedstock to bales of pulp), there are many alkaline side streams that could react with carbon dioxide to form inorganic carbonates. During the chemical pulping, the cellulose is separated from the lignin, hemicellulose, and other organic and inorganic molecules. The most common process is the Kraft process, which includes cooking the wood chips with an aqueous solution called white liquor containing sodium hydroxide and sodium sulfide [16,17]. Another interesting process, that finds application to a smaller extent, is soda pulping. In this case, the cooking reagent is a solution of only sodium hydroxide, and although it is not a widespread method, it is used for non-woody biomass such as straws or oat husks [18]. After cooking, the cellulose pulp is purified in a series of bleaching steps. A side stream of the cooking, known as weak black liquor, goes through an evaporation process to increase its solids content. The resulting high-solids slurry is called black liquor. It consists of polysaccharides, lignin, silica, inorganic chemicals from the white liquor, and various other compounds coming from the biomass. Currently, the black liquor is burned in a reactor called recovery boiler to generate energy [19]. The leftovers from this process are treated further to recover the cooking chemicals.

Liquor coming from the soda pulping of non-woody materials contains 0–36% lignin (% dry weight) and other organic compounds such as hemicelluloses, soap, saccharides, etc. It can also contain 0.4–16% silica (% dry weight) and 1–8 g/L of inorganic materials (almost exclusively sodium hydroxide and sodium carbonate) [18,20,21]. Its composition varies largely depending on the biomass, and it is highly alkaline, with a pH in the range of 12–14, owing to the addition of sodium hydroxide during the cooking process. Therefore, a potential use for it—which to the best of the authors' knowledge has not been studied until now——would be for the absorption of carbon dioxide via carbonation. The dissolved sodium hydroxide will react with carbon dioxide according to the following chemical equations leading to the formation of carbonate and bicarbonate ions [22].

$$2Na^+ + 2OH^- + CO_2 \leftrightarrow 2Na^+ + CO_3^{2-} + H_2O \tag{1}$$

$$Na^+ + OH^- + CO_2 \leftrightarrow Na^+ + HCO_3^- \tag{2}$$
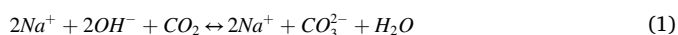
In this manner, carbon dioxide can be chemically absorbed by the liquor in the form of carbonates. In fact, sparging carbon dioxide through black liquor is not new. It has been previously considered to lower the pH of black liquor for the precipitation of lignin and silica [23–28]. Most commonly, lignin is precipitated by sparging carbon dioxide through the black liquor until the pH is lowered to 10 or 9 and then further acidification is carried out with a stronger acid, typically H_2SO_4. Heating is also applied to promote the clustering of lignin [24]. However, this technology has never been investigated for the purpose of carbon dioxide absorption.

This novel study proposes, for the first time, the use of black liquor obtained from the soda-pulping treatment of oat husks to capture carbon dioxide. Furthermore, the authors have conducted a detailed physico-chemical characterization of the carbonation product, called here carbonated black liquor. After the absorption of carbon dioxide, the carbonated black liquor could undergo different routes toward the regeneration of pure gaseous carbon dioxide or the recovery of carbonates. Fig. 1 shows two potential routes that could be followed once the black liquor has been carbonated. Nonetheless, the management of carbonated black liquor is not discussed here. The focus of this research has been on the carbonation reactions that occur between the black liquor and gaseous carbon dioxide inside a laboratory-scale bubble column.

2. Materials and methods

The experiments were conducted using weak black liquor which was prepared as follows. Oat husks, which were used as received, were subjected to prehydrolysis to loosen the lignocellulosic structure and leach some of the hemicellulose out of the material. During this process, the raw material was immersed in a weak acid inside a 1.5 L steel autoclave which rotated at a speed of 15 rpm, at 160 °C [29]. Following that, the pretreated husks were washed thoroughly with deionized water until the pH of the washing water was neutral. Finally, the soda pulping process was used to extract the pulp from the rest of the material. The pretreated material was added again to the same autoclave together with an aqueous solution of 4% w/w of sodium hydroxide and was rotated at the same speed at 170 °C for 2 h [30]. After cooking, the product was filtered to separate the pulp from the weak black liquor. The dry solid weight of the liquor was determined by drying it in an oven at 50 °C. The composition of the black liquor is presented in Table 1.

A commercial anti-foaming agent from BIM Kemi (Stenkullen, Sweden) was added to the black liquor to reduce foaming during the gas sparging. Screening of various concentrations of the agent was conducted. The concentration of 0.043 g of anti-foamer/L of black liquor proved to produce the least amount of foam. The gas used for the carbonation experiments was a mixture of 30% carbon dioxide and 70% nitrogen.
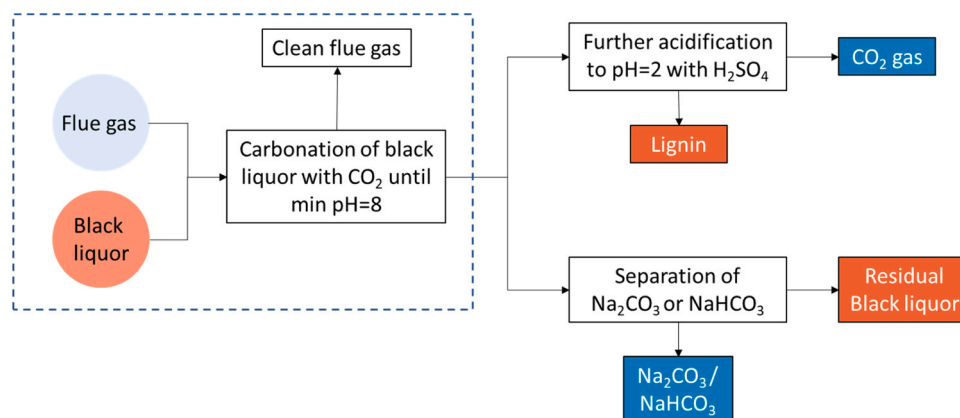

Fig. 1. Schematic representation of black liquor utilization for carbon dioxide capture. The first segment of the process contains the carbonation reaction. Once the black liquor has been carbonated to a minimum pH of 8, the product could then be acidified to recover pure carbon dioxide and the precipitated lignin. Alternatively, the carbonates could be separated from the residual liquor and the latter can be utilized as a fuel or source of chemicals.

Table 1

Composition of the oat husk black liquor used in the experiments.

Composition	Amount (% w/w)
Total solids (TS)	8
Compounds (in TS)	
Klason lignin	19.4
Acid soluble lignin	6.4
Glucose	0.3
Xylose	0.1
Elements	**Amount (ppm)**
Sodium	20,951.4
Silicon	1440.2

2.1. Carbonation reactions

The experimental setup is shown in Fig. 2. The carbonation reactions were conducted in a stirred glass reactor at ambient temperature and pressure. The gas flow was 200 mL/min. A glass sparger (DURAN) was used to sparge the gas through 100 mL of black liquor. The gas flow entered the reactor from the bottom. A mechanical stirrer (EUROSTAR Power Control-Visc Stirrer, IKA®) was immersed in the liquid, rotating at 700 rpm. Stirring was necessary to break the foam forming due to the gas sparging, and it also dispersed the gas bubbles in the liquid to enhance the carbon dioxide absorption. The foam bubbles followed the fluid motion due to the stirring, breaking once in contact with the stirring blades. The anti-foaming agent aided in producing a less dense foam. In order to monitor the carbonation process, a pH meter (HQ430D, HACH) and an FTIR (ReactIR 702 L, Mettler Toledo) analyzer were fixed in the reactor for in-line measurement. Both instruments measured every 10 s to get a detailed view of the progress of the reaction.

This setup was used to monitor the formation of carbonate and bicarbonate ions based on the pH value and FTIR absorbance spectra. According to the literature, the carbon dioxide dissolved in an aqueous solution of sodium hydroxide can exist in the form of carbonate ions, bicarbonate ions, or as carbonic acid, depending on the pH [31]. The latter species starts to appear at a pH of around 8 and since carbonic acid has very little solubility in aqueous systems, its appearance indicates that any carbon dioxide absorbed at lower pH would be released again in the atmosphere. For this reason, it was decided to consider the pH of 8 as the threshold upon which the carbonation was regarded as completed.

2.2. Carbon dioxide absorption capacity

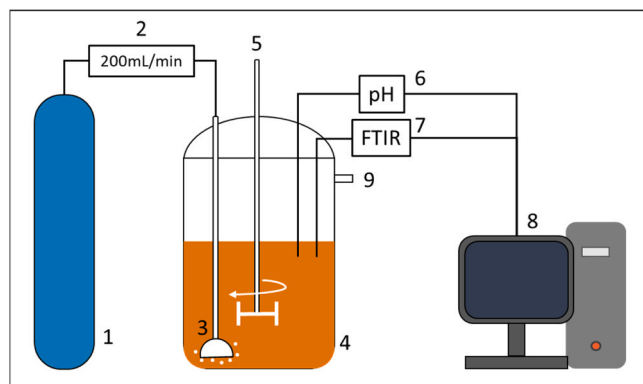The setup shown in Fig. 2 was used to follow the reactions happening

Fig. 2. Experimental setup of black liquor carbonation. 1) Gas bottle with 30% carbon dioxide and 70% nitrogen. 2) Mass flow controller with a set flow at 200 mL/min. 3) Sparger. 4) Reactor with 100 mL capacity. 5) Mechanical stirrer set at 700 rpm. 6) pH meter. 7) FTIR analyzer. 8) In-line data lodger. 9) Gas outlet.

with time. The experiment was conducted in triplicate, and the time required to reach a pH of 8 was noted for each one. The average duration of these experiments was calculated. Then experiments of the same duration were carried out to determine the absorption capacity. This was done by measuring the weight before and after with an analytical balance (QUINTIX2102–1S, Sartorius). The weight increase of the reactor after the carbonation corresponded directly to the amount of carbon dioxide captured in the black liquor. The pH of the liquor was also measured before and after the experiment to ensure that the carbonation had reached completion within the duration of the experiment, based on the criterion of a pH of 8. Triplicate experiments were conducted to ensure the reproducibility of the results. In addition, black experiments were also conducted by sparging pure nitrogen through black liquor at the same experimental conditions to account for evaporation losses. The rate of weight loss due to evaporation was 0.005 g/min.

2.3. Physicochemical characterization

Liquid state ^{13}C NMR was recorded on a Bruker Avance III HD (700 MHz ^1H) equipped with a QCI cryoprobe. Samples of black liquor before and after carbonation were transferred to an NMR tube, and a small amount of D_2O (Sigma, 99.8% D) was added to lock and shim the sample. A z-restored spin-echo pulse sequence was used with 8192 scans and a repetition time of 0.1 s [32]. An exponential window function of 20 Hz was applied before the baseline correction.

After reaching a pH of 8, the carbonated black liquor samples were divided in two. One part was filtered using filter paper number 3 (Munktell), to separate the precipitated solids from the rest of the liquid. Then both the residue and the filtrate were left in an oven at 70 °C for two days to dry. The second part, as well as a sample of non-carbonated black liquor were also dried in the oven without previous treatment. After drying, the solid samples were examined with an optical microscope (ZEISS SteREO Discovery.V12) and a scanning electron microscope (SEM – Phenom ProX, ThermoFisher Scientific). Powder X-ray diffraction analysis (XRD – D8 Discover, Bruker) was performed after grinding the dried samples into a fine powder. The XRD spectra were recorded using the software DIFFRAC.EVA V5.2 and the Crystallography Open Database was used to analyze the spectra.

2.4. Computational fluid dynamics

Through computational fluid dynamics (CFD) simulations, this section aims to illustrate the mixing characteristics in an agitated vessel (corresponding to the experimental setup mentioned in Section 2.1) between the dispersed bubbly flow and the continuous liquid phase. Fig. 3A illustrates a three-dimensional (3D) schematic representation of the model used for the simulations. The bubbly phase was injected through a sparger, shown in blue on the left. To achieve adequate mixing between the gas and liquid phases, the impeller rotated at speed $\Omega = 700$rpm, with respect to the z-axis (the reactor axis of symmetry). The Eulerian-Eulerian approach was adopted for the gas-liquid flow, and both phases were considered interpenetrating continua [33,34]. The impeller region was modeled with the Multiple-Reference-Frame (MRF) method in a rotating frame of reference, and the rest of the vessel was in a stationary frame of reference.

The turbulence modeling employed the standard $k - \varepsilon$ two equations model with enhanced wall treatment. The bubble-induced turbulence was considered by adding a source term in the momentum equation [35]. The models for interfacial forces of drag, shear lift, wall lift, turbulent dispersion, and virtual mass forces are summarized in Table 2 [36,37].

As shown in Fig. 3B, the generated grid was of mosaic type with a hexahedral-dominant topology. A grid-independent solution was obtained for about 1.18×10^6 cells considering four mesh refinement levels and monitoring several key performance parameters such as the
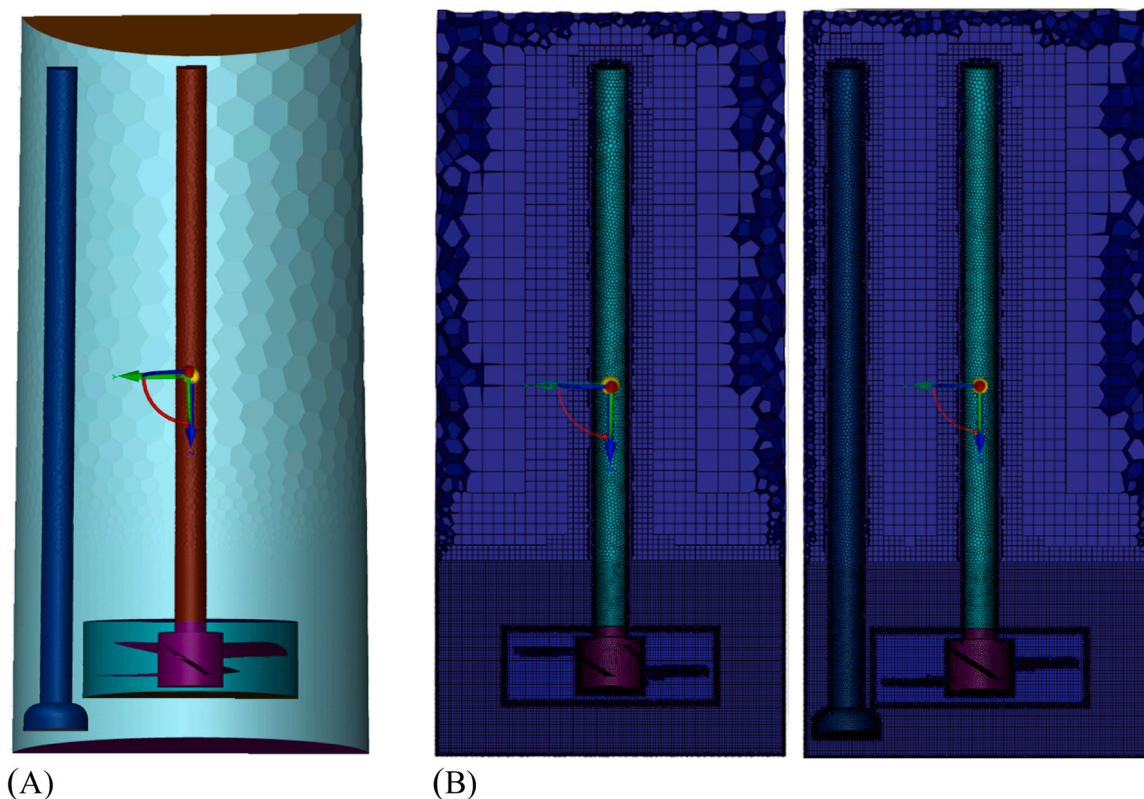
Fig. 3. (A) 3D schematic representation of the reactor with sparger and the impeller and (B) the generated mosaic grid with a hexahedral dominant mesh topology.

Table 2

Summary of the models employed for the interfacial forces between the dispersed gaseous phase and the continuous liquid phase.

Force	References
Drag	Ishii and Zuber.[38]
Shear lift	Tomiyama et al.[39]
Wall lift	Lubchenko et al.[40]
Turbulent dispersion	Burns et al.[41]
Virtual mass	Constant coefficient $C_{vm} = 0.5$[42]

gas volume fraction and liquid mean velocity. The model was solved using ANSYS FLUENT (Version 2022 R2) based on a control-volume approach. At the inlet of the sparger (bottom surface), the velocity of the liquid phase was zero, while the superficial gas velocity was $U_{GS} = 29.47$ mm·s^{-1} with a gas volume fraction of $\alpha_G = 1.0$. The no-slip boundary condition was applied for all vessel walls, shafts, impellers, and sparger surfaces. The degassing boundary condition was used at the top of the reactor allowing only the gas phase to escape. At the low solid volume fractions of black liquor used in the experiments, the rheological behavior of the fluid can be assumed Newtonian with a viscosity of 0.0013 Pa·s. Hence, air was treated as a secondary gaseous phase immersed in a primary liquid phase. The interfacial tension value between the two phases was set to 0.072 N·m^{-1}, and the gravitational acceleration g = 9.81 m·s^{-2} was considered in the positive z direction (the downwards direction in Fig. 3). The coupled algorithm was chosen for the velocity-pressure coupling. The second-order upwind discretization scheme was selected for the momentum equation, and the QUICK method for the volume fraction equation. The bounded second-order implicit method was considered for the transient formulation, and the convergence criterion was set to 10^{-4} for all the residuals of the transport equations. The time step was adaptive, ensuring that the global Courant–Friedrichs–Lewy number was less than unity.

3. Results and discussion

3.1. Computational fluid dynamics

The CFD study was conducted to evaluate the mixing between the two phases in the bubble column reactor. Ensuring adequate mixing is crucial to achieve an efficient carbonation process. Thus, this section precedes the experimental study. Fig. 4 depicts the liquid phase velocity vectors superimposed on the velocity magnitude. It can be observed that the impeller movement effectuates vortex formation and generates rotational areas in different planes, ensuring an appropriate degree of mixing in all directions. The liquid modulus of velocity U_L yields higher values in the MRF zone resulting in a superior mixing quality between the dispersed bubbly phase and the liquid medium, which can be confirmed by looking at the gas momentum distribution. Fig. 4A shows the iso-surface of the gas velocity $U_G = 0.3$ m·s^{-1} the presence and absence of stirring. Apparently, without the impeller rotation ($\Omega = 0$), the gas tends to rise towards the gas-liquid surface in the vicinity of the sparger, and the bubbly phase does not spread uniformly in the reactor. In contrast, with the stirring ($\Omega = 700$rpm), the impeller rotation induces a more pronounced degree of momentum dispersion and creates an enhanced mixing homogeneity of the gaseous phase.

The gas holdup is the most crucial hydrodynamic parameter for this multiphase system. Fig. 5B shows the iso-surface of the gas volume fraction $\alpha_G = 0.01$, with and without consideration of forced mixing. Similar to the flow field, it is evident from the void fraction distribution that for $\Omega = 0$rpm (without stirring), bubbles are amassed near the sparger, and the values are significantly higher in one portion of the reactor, leading to inferior mixing quality. On the contrary, we can confirm that with the impeller rotation, the radial flow induced by the impeller intervenes in bubble dynamics and intensifies the gas phase dispersion. Hence, the mixing performance is enhanced, and the gas phase is distributed more homogeneously in the vessel.
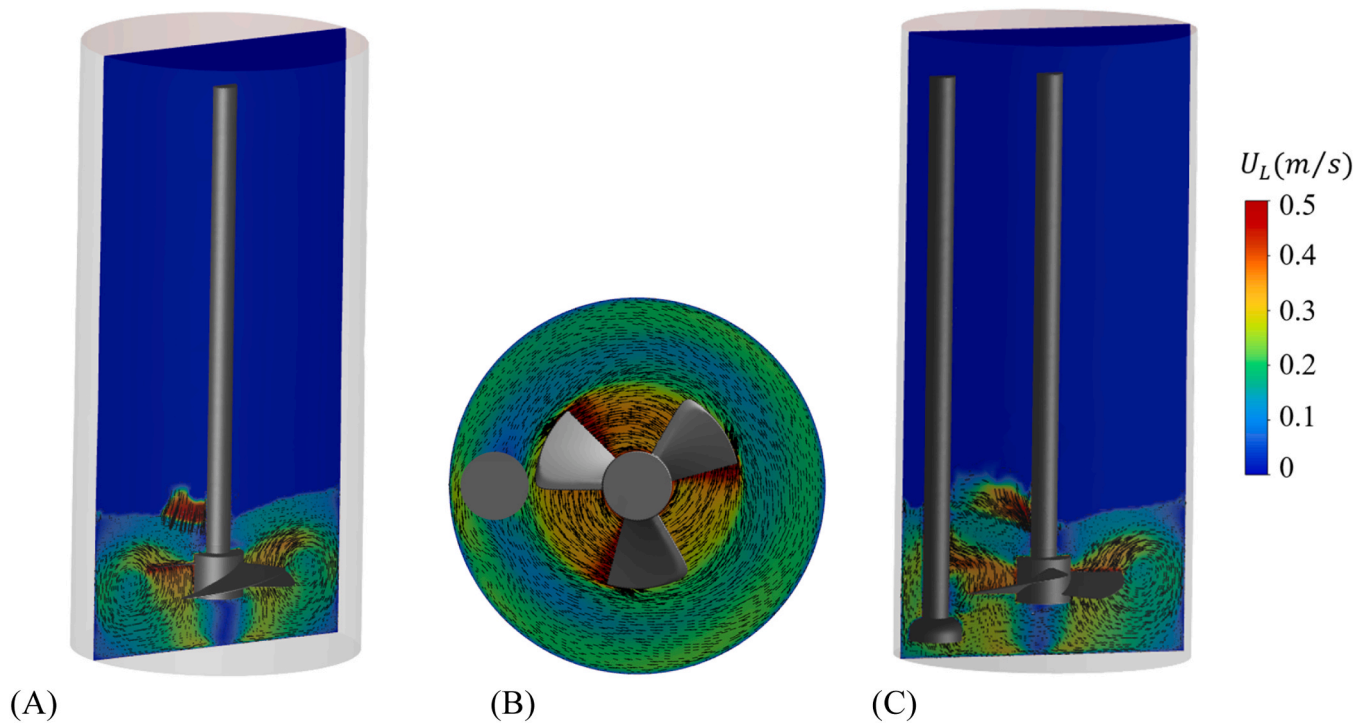
Fig. 4. The liquid velocity vector is superimposed on the liquid modulus of liquid velocity at (A) yz − plane, (B) xy − plane, and (C) xz − plane.
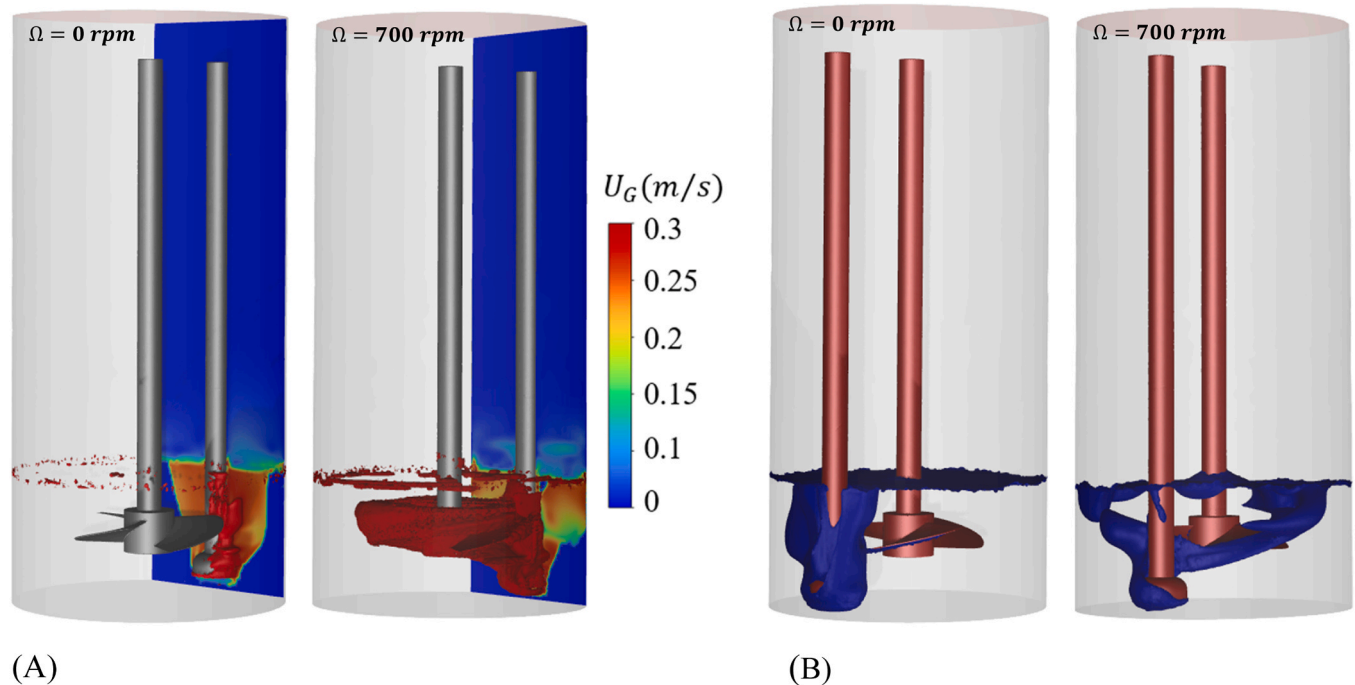

Fig. 5. (A) the iso-surface of gas modulus of velocity $U_G = 0.3$ m·s^{-1} and (B) the iso-surface of gas volume fraction $\alpha_G = 0.01$ for $\Omega = 0$ and 700rpm.

3.2. Chemical reactions of black liquor during carbonation

The pH and FTIR spectra of black liquor were monitored throughout the experiment (Fig. 6). Fig. 6A shows the evolution of the FTIR spectra with time. Sodium carbonate is known to have a characteristic absorbance at 1410 cm^{-1}, while sodium bicarbonate appears with small bands at 1300 cm^{-1} and 1000 cm^{-1} [43]. Leventaki et al. sparged carbon dioxide through aqueous solutions of sodium hydroxide, and the absorbance at around 1380 cm^{-1} was attributed to carbonate ions, while

bicarbonate ions appeared with a band of lower intensity at 1360 cm^{-1}, a shoulder at 1300 cm^{-1} and a smaller band at 1008 cm^{-1} [44]. The absorbance of water appears at around 1635 cm^{-1}. The initial spectrum of black liquor showed an intense band of water and a small band at 1390 cm^{-1}, which indicates that black liquor contains a small concentration of carbonate ions. After 10 min, the intensity of the band increased, corresponding to an increase in concentration, and after 20 min, the bicarbonate bands were also clearly visible.

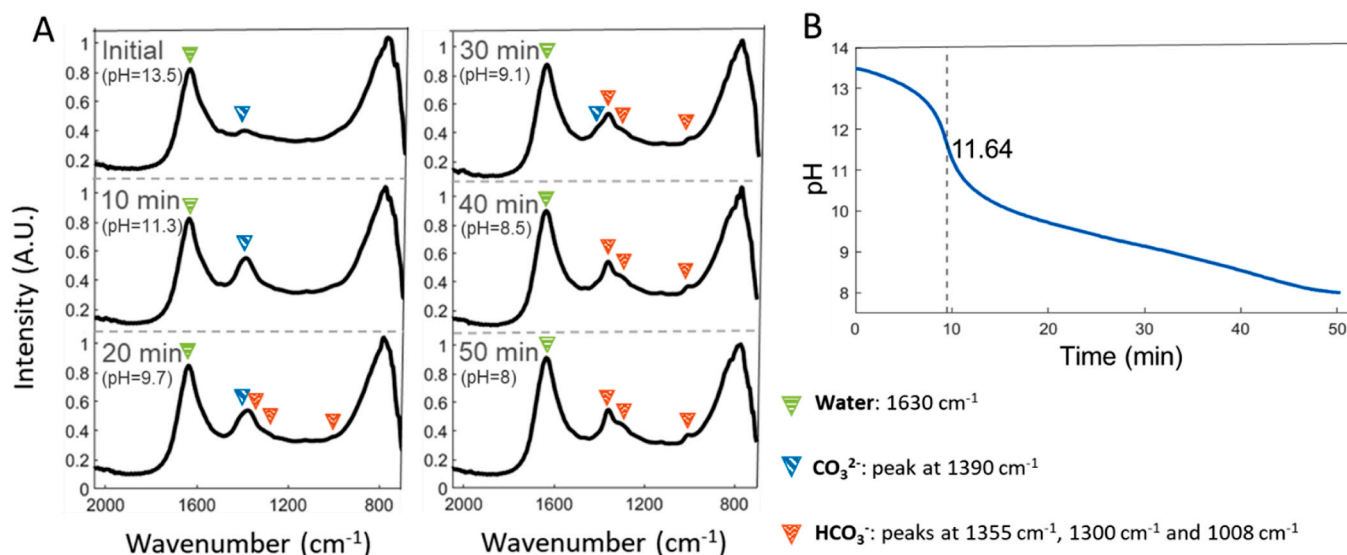The band at 1355 cm^{-1} overlaps with carbonate ions forming a

Fig. 6. (A) FTIR spectra with time during a carbonation experiment. The bands marked with a green arrow at around 1630 cm^{-1} correspond to the absorbance of water, the bands marked with a blue arrow at 1390 cm^{-1} show the carbonate ions, and the three bands in red color at 1355, 1300, and 1008 cm^{-1} are characteristic of bicarbonate ions. (B) Evolution of pH with time during the carbonation of black liquor.

broader band. After 30 min, the number of carbonate ions decreased, as indicated by the lower absorbance, while the bands of the bicarbonate species became more distinct, and at the end of the experiment, at 50 min, the presence of bicarbonates was evident. The FTIR spectra might be interpreted quantitatively under optimal circumstances. However, due to the overlapping of bands, it is unfeasible to calculate how much of each species is present. Nevertheless, since no other molecules in the black liquor had a significant absorbance in the FTIR spectrum, the analysis of the formation of carbonate and bicarbonate ions over time was clear.

The trend of the pH was also followed with time as can be seen in Fig. 6B. The initial pH of black liquor was 13.5. Within the first 6 min of the experiment, the pH decreased slowly until the value of 12.9. Nevertheless, as the pH is an expression of the logarithmic concentration of hydronium ions, this slow decrease in pH corresponds to a significant increase in the concentration of hydronium ions (or a decrease in hydroxide ions). After that, the pH dropped very quickly for around 7 min. This drastic drop halted at the pH value of 10.3. In titration, the point at which the pH decline slows down is called the endpoint, and it corresponds to the end of the reaction.

The pH value at the maximum rate of decrease is known as the equivalent point, or the point where the reactants are at the exact stoichiometric ratio based on the chemical reaction. The equivalent point, in this case, appeared at a pH of 11.64. The chemical Eq. (1) above shows the reaction that occurs at this pH range. From a previous study where carbon dioxide was sparged through a pure solution of sodium hydroxide, the equivalent point of this chemical reaction appeared at a pH of around 12.7 [44]. This indicates that in the case of black liquor, there might be other reactions also taking place, causing the equivalence point to shift. From that point, the experiment took an additional 37 min until pH 8, at which the pH reached a plateau. During this period, there is an equilibrium between carbonate and bicarbonate ions which slowly shifts to favor the formation of bicarbonate ions. The chemical reaction of Eq. (2) takes place as more carbon dioxide is sparged, but at the same time, the already formed carbonate ions are also turning into bicarbonate ions. At the pH of 8, bicarbonate ions should be the predominant species.

3.3. Capture capacity of black liquor

As mentioned before, the experiments using the pH meter and FTIR probe were conducted in triplicate to estimate the total duration of carbonation. Then the experiments were conducted for the same amount of time, and the reactor's weight was measured initially and at the end of the experiment. Table 3 shows the weight of carbon dioxide absorbed in black liquor calculated in g/L. Each of the three experiments was stopped at a pH of around 8, after which the absorption of carbon dioxide is insignificant. The average absorption capacity from the three experiments was 30.8 g of carbon dioxide/L of black liquor. According to previous findings, an aqueous solution of sodium hydroxide 3% w/w would have an absorption capacity of around 30 g of carbon dioxide/L of solution [44]. This falls in line with our finding, since the initial addition of sodium hydroxide during soda pulping was 4% w/w, but a small amount was consumed, and some was also carbonated during the cooking process.

Based on the volumetric flow of the gas, an estimation of the amount of carbon dioxide flowing into the system can be deduced as follows. The inlet gas flow was 200 mL/min with 30% of carbon dioxide and the volumetric flow of carbon dioxide was 60 mL/min. The reactor had an outlet to the atmosphere and no external heat was applied. The temperature sensor of the FTIR probe showed a range of temperatures from 23° to 27°C. The slight fluctuations of temperature can be attributed to the exothermic nature of the carbonation reaction. Therefore, the conditions at the inlet of the gas can be considered ambient (25 °C and 1 atm). The density of carbon dioxide at these conditions is 1.96 kg/m^3, given that its molar mass is 44.01 g/mol and assuming that carbon dioxide is an ideal gas [45]. So the mass flow of carbon dioxide was 0.118 g/min, which, for 50 min of reaction corresponds to 5.9 g of carbon dioxide. Thus, one can conclude that roughly half of the carbon dioxide that entered the system was absorbed. For the purpose of designing a flue gas cleaning process using this material as the absorbent, the system would have to be optimized. The volumetric ratio between black liquor and gas flow should be increased to ensure that the outlet gas is as clean as possible. Additionally, although this study was conducted in a semi-batch reactor, perhaps a continuous reactor would

Table 3
Absorption capacity of carbon dioxide in black liquor.

Experiment No	Final pH	Absorption Capacity (g/L)
1	7.96	32.9
2	8.05	29.3
3	8.04	30.3

be more efficient for this process. Nevertheless, providing information about the capture capacity of black liquor is crucial for the design of an industrial reactor. Here the capture capacity of black liquor from oat husks was obtained, but different types of black liquor will have different capacities, depending on the cooking chemicals, solids content and composition. This must be considered for upscaling the process.

3.4. Physicochemical characterization

The NMR spectra of black liquor before and after carbonation are presented in Fig. 7, showing a complex mixture of molecules. The aromatic part of lignin should be visible in the region between 100 and 120 ppm and the methoxy groups around 50 ppm. The peaks in the region between 50 and 100 ppm arise most likely from hemicelluloses. However, the NMR spectrum for the black liquor before carbonation (Fig. 7A) shows almost no lignin peaks. This might be due to the low amount of lignin. The peak at 168 ppm corresponds to carbonate ions confirming that the non-carbonated black liquor contains a small amount of carbonate ions which agrees with the FTIR results. After carbonation at pH 8, there was no considerable change in the organic molecules' composition (Fig. 7B). However, the carbonate peak disappeared, and another more intense peak at 161 ppm corresponding to bicarbonate ions appeared [46]. This indicates that the black liquor has been carbonated, and the dominant species are bicarbonates which is reasonable at pH 8.

The XRD diffractograms of black liquor before and after carbonation are presented in Fig. 8. Black liquor without carbonation resulted in a diffractogram with a few high peaks that could not be identified. Black liquor contains a huge variety of organic and inorganic compounds that might change upon drying, forming crystalline and/or amorphous structures. However, after carbonation and filtration, the signal became more defined, and some characteristic signals could be observed. In the case of the residue of carbonated black liquor, the broad, low-intensity band that appeared in the angle range of 18–29º (Fig. 8B) corresponds to precipitated amorphous silica, as observed in previous literature [47]. In the highly alkaline black liquor, silica reacts with hydroxide ions to form soluble silicate ions. Silicate ions turn into insoluble silica at a pH range of 8–10, while lignin, which has a more complicated mechanism of protonation, reaches maximum precipitation at a pH of around 2–3 [47,48]. Most likely, the broad band in the XRD diffractogram arises from precipitated silica and, to a smaller extent, from amorphous lignin. Within the angle range of 32–60º other small peaks could be observed. Based on the Figure of Merit (FOM) calculated in the XRD software, these peaks had a 30% match to the signal of sodium carbonate. The FOM percentages given in Fig. 8 do not provide quantitative information. They express how well the peaks of the recorded signal fit to the diffractograms of model molecules stored in the Crystallography Open Database.

The diffractogram of the filtrate of carbonated black liquor displayed a stronger indication of sodium hydroxide and, to a lesser degree, sodium bicarbonate. This result contradicts the NMR and FTIR data, which showed a predominance of bicarbonate ions in the carbonated black liquor. The conversion of the bicarbonate species back into carbonate could be attributed to the drying method. Sodium bicarbonate decomposes to sodium carbonate at a starting temperature of 80 °C [49]. As the samples were dried in the oven at 70 °C over the course of a few days, it is possible that the bicarbonate species decomposed to some extent and solidified into sodium carbonate. Therefore, an increase in temperature in the post-treatment of carbonated black liquor leads to sodium bicarbonate decomposition, which would result in a slight release of carbon dioxide. This raises the important point that if the goal of the process is maximum absorption of carbon dioxide, heating should be avoided.

The dried samples were also studied with an optical microscope (Fig. 9). Fig. 9A and B show the non-carbonated black liquor and the residue of the filtration, respectively, and Fig. 9C shows the filtrate after carbonation. In Fig. 9C, white particles appeared, which did not exist in the other two samples. This, along with the XRD diffractograms, allows us to assume that the white crystals are composed of a mixture of sodium carbonate and sodium bicarbonate. There were no visible crystals in the residue of the filtration, which is also confirmed by the XRD diffractograms. This is because sodium bicarbonate is soluble in aqueous systems, so, during the filtration, almost all the sodium and bicarbonate ions would be filtered through.

During the filtration process, it is possible that as the residue was becoming more condensed, the concentration of sodium bicarbonate exceeded its solubility limit so that a very small concentration could have been solidified and stayed trapped in the residue. The sodium bicarbonate would then decompose into sodium carbonate during the drying process, and that would explain the XRD peaks that appeared with low intensity in Fig. 8B. However, as the concentration of the sodium carbonate in the residue is very low, no crystals were present in the images. These findings were confirmed with SEM (Fig. 10). The images in Fig. 10A and B correspond to black liquor before carbonation and to the residue after the carbonation. The filtrate of the carbonated black liquor exhibited small crystalline particles (Fig. 10C, D) which were not there before the carbonation or in the residue.

4. Conclusions

We showed that black liquor could be used for the chemical absorption of carbon dioxide in a bubble column reactor. Foaming was reduced by stirring and adding a commercial anti-foamer. Initially, as carbon dioxide was sparged through the liquid, carbonate ions formed. As the pH dropped, bicarbonate ions started forming. At the final pH of 8, bicarbonate ions were the most abundant species, which was confirmed by FTIR and ^{13}C NMR. During the reaction, lignin and silica precipitated. After drying the solids and the liquid phase, carbonates and amorphous silica were found. The flow field for the bubble column reactor was investigated using transient multiphase 3D-CFD simulations, and it was shown that the employed sparger-impeller combination could provide adequate mixing between the dispersed bubbly phase and the liquid phase.

The absorption capacity of the black liquor was found to be around 30 g of carbon dioxide/L of black liquor. This result will vary depending on the amount of sodium hydroxide and the overall composition of black liquor. Our results indicate that not only sodium hydroxide is involved in carbon dioxide absorption. Hence, further research is needed to study the effect of black liquor composition on its absorption capacity. For this purpose, other types of black liquor should also be tested in the future, both coming from the soda pulping and the Kraft process. In addition, further investigation must be conducted to evaluate the potential paths of the carbonated black liquor—valorization of the precipitated
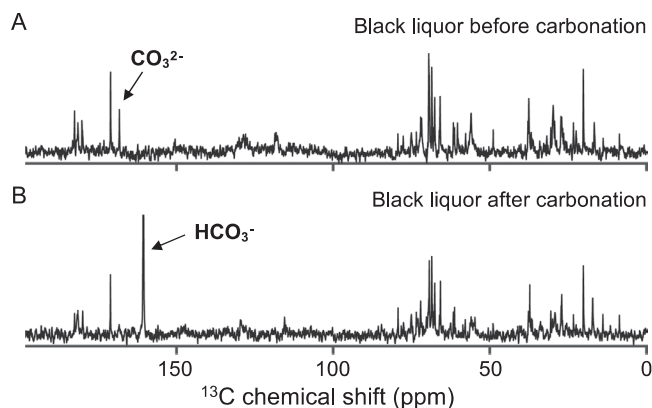
Fig. 7. Liquid state ^{13}C NMR spectra of black liquor before carbonation (A) and after carbonation (B).
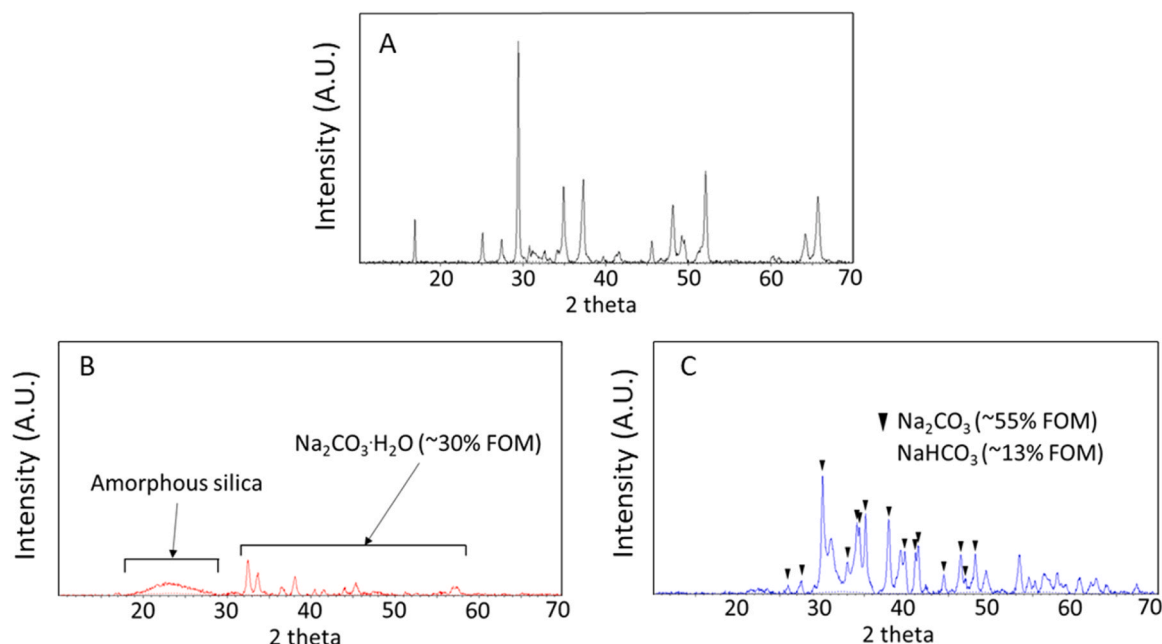
Fig. 8. XRD diffractograms of black liquor (A), non-carbonated residue from the filtration of carbonated black liquor (B), and filtrate from the filtration of carbonated black liquor (C). The Figure of Merit (FOM) displayed in (B) and (C) is an indication of how much the signal matches with that of a particular molecular structure from the Crystallography Open Database.
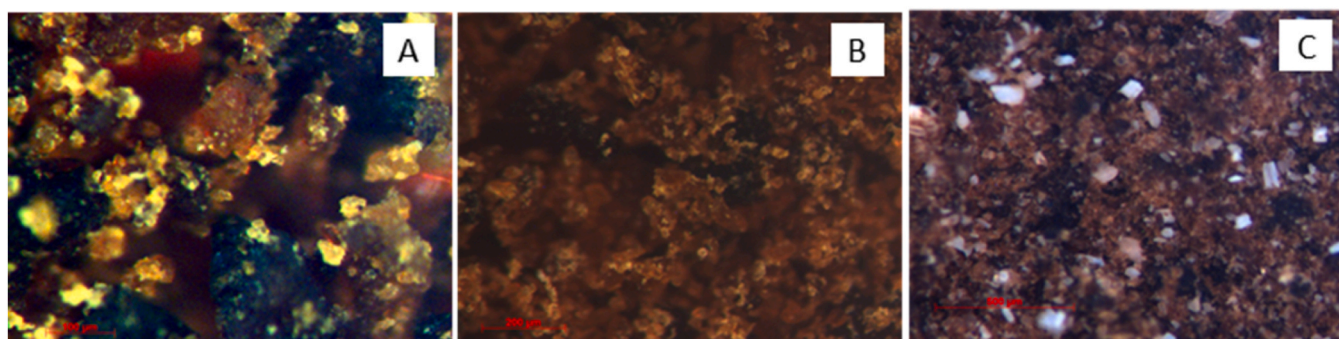

Fig. 9. Optical microscope images of (A) non-carbonated black liquor, (B) residue from the filtration of carbonated black liquor, and (C) filtrate from the filtration of carbonated black liquor.

products and regeneration. By lowering the pH during carbonation silica can be precipitated and removed. This is a great benefit as high silica content causes problems in the recovery boiler. Regeneration of carbon dioxide is possible also by lowering the pH to an appropriate acidic level. The amount and purity of the generated carbon dioxide could also be a point of study. The resulting liquor could then either be treated to separate the lignin or proceed to the recovery boiler for energy production.

The present work is an important first step towards the utilization of black liquor for carbon dioxide capture and the understanding of the carbonation reactions in this system. This study sheds light on the absorption mechanism of carbon dioxide in black liquor as well as the physicochemical properties of the final product. In addition, detailed research was conducted on the development of a computational model that can evaluate the mixing of the flows in a bubble column reactor. This type of model can prove valuable for the optimization and up-scaling of bubble column reactors for the absorption of carbon dioxide on an industrial scale. The authors provided a scientific foundation of this concept to be further investigated in depth and bring forward new ideas.

CRediT authorship contribution statement

Emmanouela Leventaki: Conceptualization, Data curation, Formal analysis, Investigation, Methodology, Validation, Visualization, Writing – original draft, Writing – review & editing. **Francisco M. Baena-Moreno:** Conceptualization, Investigation, Methodology, Supervision. **Joanna Wojtasz-Mucha:** Investigation. **Niclas Sjöstedt:** Investigation. **Abdul Raouf Tajik:** Methodology, Software, Data curation, Formal analysis, Investigation, Visualization. **Gaetano Sardina:** Project administration, Supervision. **Henrik Ström:** Funding acquisition, Project administration, Supervision. **Diana Bernin:** Conceptualization, Funding acquisition, Project administration, Resources, Supervision, Visualization.

Declaration of Competing Interest

The authors declare that no financial interests/personal relationships need to be considered as potential competing interests.
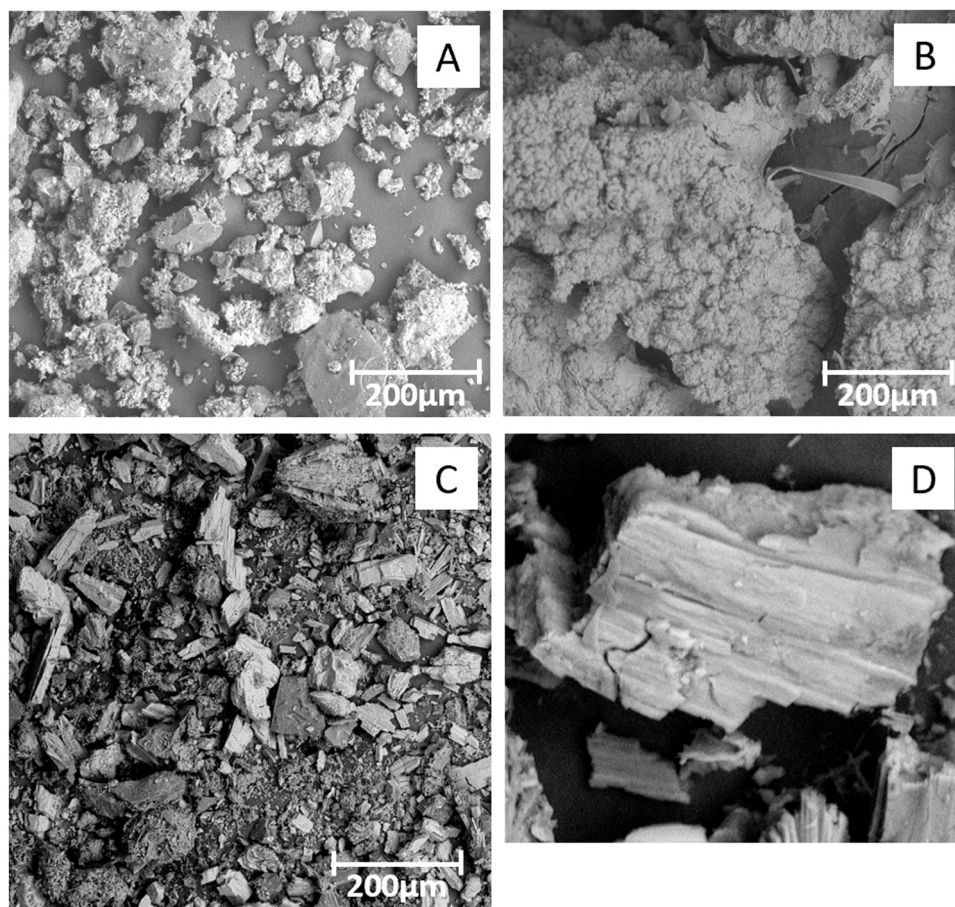
Fig. 10. SEM images of (A) non-carbonated black liquor, (B) residue from the filtration of carbonated black liquor, (C) filtrate from the filtration of carbonated black liquor, and (D) zoomed-in image of crystal from the filtrate.

Data availability

Data will be made available on request.

Acknowledgments

References

[1] Global Warming of 1.5°C an IPCC special report on the impacts of global warming of 1.5 °C above pre-industrial levels and related global greenhouse gas emission pathways, in the context of strengthening the global response to the threat of climate change, sustainable development, and efforts to eradicate poverty, 2018.

[2] K.S. Ng, N. Zhang, J. Sadhukhan, Techno-economic analysis of polygeneration systems with carbon capture and storage and CO_2 reuse, Chem. Eng. J. 219 (2013) 96–108, https://doi.org/10.1016/j.cej.2012.12.082.

[3] Z. Zhang, S.-Y. Pan, H. Li, J. Cai, A.G. Olabi, E.J. Anthony, V. Manovic, Recent advances in carbon dioxide utilization, Renew. Sustain. Energy Rev. 125 (2020), 109799, https://doi.org/10.1016/j.rser.2020.109799.

[4] I.M.S. Anekwe, E.K. Tetteh, S. Akpasi, S.J. Atuman, E.K. Armah, Y.M. Isa, Carbon dioxide capture and sequestration technologies – current perspective, challenges and prospects, in: Green Sustainable Process for Chemical and Environmental Engineering and Science, Elsevier, 2023, pp. 481–516, https://doi.org/10.1016/B978-0-323-99429-3.00034-5.

[5] F.M. Baena-Moreno, E. Leventaki, A. Riddell, J. Wojtasz-Mucha, D. Bernin, Effluents and residues from industrial sites for carbon dioxide capture: a review, Environ. Chem. Lett. (2022), https://doi.org/10.1007/s10311-022-01513-x.

[6] S.-Y. Pan, E.E. Chang, P.-C. Chiang, CO_2 capture by accelerated carbonation of alkaline wastes: a review on its principles and applications, Aerosol Air Qual. Res 12 (2012) 770–791, https://doi.org/10.4209/aaqr.2012.06.0149.

[7] V. Romanov, Y. Soong, C. Carney, G.E. Rush, B. Nielsen, W. O'Connor, Mineralization of carbon dioxide: a literature review, ChemBioEng Rev. 2 (2015) 231–256, https://doi.org/10.1002/cben.201500002.

[8] W. Liu, L. Teng, S. Rohani, Z. Qin, B. Zhao, C.C. Xu, S. Ren, Q. Liu, B. Liang, CO_2 mineral carbonation using industrial solid wastes: A review of recent developments, Chem. Eng. J. 416 (2021) 129093, https://doi.org/10.1016/j.cej.2021.129093.

[9] M. Tu, H. Zhao, Z. Lei, L. Wang, D. Chen, H. Yu, T. Qi, Aqueous Carbonation of Steel Slag: A Kinetics Study, ISIJ Int. 55 (2015) 2509–2514, https://doi.org/10.2355/isijinternational.ISIJINT-2015-142.

[10] S.K. Kaliyavaradhan, T.-C. Ling, Potential of CO_2 sequestration through construction and demolition (C&D) waste—An overview, J. CO_2 Util. 20 (2017) 234–242, https://doi.org/10.1016/j.jcou.2017.05.014.

[11] C.J. Engelsen, J. Mehus, C. Pade, D.Henning Saether, Carbon dioxide uptake in demolished and crushed concrete, Oslo (2005).

[12] A.C. Spínola, C.T. Pinheiro, A.G.M. Ferreira, L.M. Gando-Ferreira, Mineral carbonation of a pulp and paper industry waste for CO_2 sequestration, Process Saf. Environ. Prot. 148 (2021) 968–979, https://doi.org/10.1016/j.psep.2021.02.019.

[13] R. Sun, Y. Li, C. Liu, X. Xie, C. Lu, Utilization of lime mud from paper mill as CO_2 sorbent in calcium looping process, Chem. Eng. J. 221 (2013) 124–132, https://doi.org/10.1016/j.cej.2013.01.068.

[14] R. Pérez-López, G. Montes-Hernandez, J.M. Nieto, F. Renard, L. Charlet, Carbonation of alkaline paper mill waste to reduce CO_2 greenhouse gas emissions into the atmosphere, Appl. Geochem. 23 (2008) 2292–2300, https://doi.org/10.1016/j.apgeochem.2008.04.016.

[15] A. Santos, A. Barbosa-Póvoa, A. Carvalho, Life cycle assessment of pulp and paper production – A Portuguese case study, Comput. Aided Chem. Eng. (2018) 809–814, https://doi.org/10.1016/B978-0-444-64235-6.50142-X.

[16] L. Simão, D. Hotza, F. Raupp-Pereira, J.A. Labrincha, O.R.K. Montedo, Wastes from pulp and paper mills - a review of generation and recycling alternatives, Cerâmica 64 (2018) 443–453, https://doi.org/10.1590/0366-69132018643712414.

[17] P. Bajpai, Pulping Fundamentals, in: Biermann's Handbook of Pulp and Paper, Elsevier, 2018, pp. 295–351, https://doi.org/10.1016/B978-0-12-814240-0.00012-4.

[18] M.A. Azeez, Pulping of Non-Woody Biomass, in: Pulp and Paper Processing, InTech, 2018, https://doi.org/10.5772/intechopen.79749.

[19] E. Vakkilainen, Kraft recovery boilers – Principles and practice, 2003.

[20] D.M. Le, H.R. Sørensen, N.O. Knudsen, A.S. Meyer, Implications of silica on biorefineries - interactions with organic material and mineral elements in grasses, Biofuels, Bioprod. Bioref. 9 (2015) 109–121, https://doi.org/10.1002/bbb.1511.

[21] J.C. Solarte-Toro, J.A. Arrieta-Escobar, B. Marche, C.A. Cardona Alzate, Effect of the lignin extraction process on the economics of a woody-based biorefinery, in: 2021: pp. 1871–1876. https://doi.org/10.1016/B978-0-323-88506-5.50290-4.

[22] D.A. Wolf-Gladrow, R.E. Zeebe, C. Klaas, A. Körtzinger, A.G. Dickson, Total alkalinity: The explicit conservative expression and its application to biogeochemical processes, Mar. Chem. 106 (2007) 287–300, https://doi.org/10.1016/j.marchem.2007.01.006.

[23] J. Velez, M.C. Thies, Temperature Effects on the Molecular Properties of Liquid Lignin Recovered from Kraft Black Liquor, ACS Sustain Chem. Eng. 3 (2015) 1032–1038, https://doi.org/10.1021/sc500703m.

[24] L. Kouisni, P. Holt-Hindle, M. Paleologou, K. Maki, The lignoforce system™: a new process for the production of high-quality lignin from black liquor, J. Sci. Technol. For. Prod. Process. 2 (2012).

[25] M.A. Hubbe, R. Alén, M. Paleologou, M. Kannangara, J. Kihlman, Lignin recovery from spent alkaline pulping liquors using acidification, membrane separation, and related processing steps: a review, Bioresources 14 (2019).

[26] H. Wallmo, H. Theliander, T. Richards, Lignin precipitation from kraft black liquors: kinetics and carbon dioxide absorption, Pap. Timber 89 (2007).

[27] Bertel Myreen, Process for recovering alkali and black liquor containing silicatae, US6183598B1, 2001.

[28] T. Sewring, J. Durruty, L. Schneider, H. Schneider, T. Mattsson, H. Theliander, Acid Precipitation of Kraft Lignin from Aqueous Solutions: The Influence of pH, Temperature, and Xylan, J. Wood Chem. Technol. 39 (2019) 1–13, https://doi.org/10.1080/02773813.2018.1488870.

[29] J. Behin, M. Zeyghami, Dissolving pulp from corn stalk residue and waste water of Merox unit, Chem. Eng. J. 152 (2009) 26–35, https://doi.org/10.1016/j.cej.2009.03.024.

[30] C. Heitner, D. Dimmel, J. Schmidt, Lignin and Lignans: Advances in Chemistry, CRC Press,, 2016.

[31] D.A. Wolf-Gladrow, R.E. Zeebe, C. Klaas, A. Körtzinger, A.G. Dickson, Total alkalinity: The explicit conservative expression and its application to biogeochemical processes, Mar. Chem. 106 (2007) 287–300, https://doi.org/10.1016/j.marchem.2007.01.006.

[32] Y. Xia, S. Moran, E.P. Nikonowicz, X. Gao, Z-restored spin-echo13C 1D spectrum of straight baseline free of hump, dip and roll, Magn. Reson. Chem. 46 (2008) 432–435, https://doi.org/10.1002/mrc.2195.

[33] X. Guan, X. Li, N. Yang, M. Liu, CFD simulation of gas-liquid flow in stirred tanks: Effect of drag models, Chem. Eng. J. 386 (2020), 121554, https://doi.org/10.1016/j.cej.2019.04.134.

[34] G. Montante, A. Paglianti, F. Magelli, Experimental analysis and computational modelling of gas–liquid stirred vessels, Chem. Eng. Res. Des. 85 (2007).

[35] B. Magolan, N. Lubchenko, E. Baglietto, A quantitative and generalized assessment of bubble-induced turbulence models for gas-liquid systems, Chem. Eng. Sci.: X 2 (2019), 100009, https://doi.org/10.1016/j.cesx.2019.100009.

[36] N. Lubchenko, B. Magolan, R. Sugrue, E. Baglietto, A more fundamental wall lubrication force from turbulent dispersion regularization for multiphase CFD applications, Int. J. Multiph. Flow. 98 (2018) 36–44, https://doi.org/10.1016/j.ijmultiphaseflow.2017.09.003.

[37] O. Marfaing, M. Guingo, J. Laviéville, S. Mimouni, E. Baglietto, N. Lubchenko, B. Magolan, R. Sugrue, B.T. Nadiga, Comparison and uncertainty quantification of two-fluid models for bubbly flows with NEPTUNE_CFD and STAR-CCM+, Nucl. Eng. Des. 337 (2018) 1–16, https://doi.org/10.1016/j.nucengdes.2018.05.028.

[38] M. Ishii, N. Zuber, Drag coefficient and relative velocity in bubbly, droplet or particulate flows, AIChE J. 25 (1979) 843–855, https://doi.org/10.1002/aic.690250513.

[39] A. Tomiyama, H. Tamai, I. Zun, S. Hosokawa, Transverse migration of single bubbles in simple shear flows, Chem. Eng. Sci. 57 (2002) 1849–1858, https://doi.org/10.1016/S0009-2509(02)00085-4.

[40] N. Lubchenko, B. Magolan, R. Sugrue, E. Baglietto, A more fundamental wall lubrication force from turbulent dispersion regularization for multiphase CFD applications, Int. J. Multiph. Flow. 98 (2018) 36–44, https://doi.org/10.1016/j.ijmultiphaseflow.2017.09.003.

[41] A.D. Burns, J.-M. Shi, T. Frank, I. Hamill, The Favre Averaged Drag Model for Turbulent Dispersion in Eulerian Multi-Phase Flows Numerical analysis of thermo-acoustic gas mixture separation processes View project Co-Combustion View project The Favre Averaged Drag Model for Turbulent Dispersion in Eulerian Multi-Phase Flows, 2004. ⟨https://www.researchgate.net/publication/261761053⟩.

[42] J. Magnaudet, M. Rivero, J. Fabre, Accelerated flows past a rigid sphere or a spherical bubble. Part 1. Steady straining flow, J. Fluid Mech. 284 (1995) 97–135, https://doi.org/10.1017/S0022112095000280.

[43] National Institute of Standards and Technology NIST Chemistry WebBook Available online: http://webbook.nist.gov, (n.d.).

[44] E. Leventaki, F.M. Baena-Moreno, G. Sardina, H. Ström, E. Ghahramani, S. Naserifar, P.H. Ho, A.M. Kozlowski, D. Bernin, In-Line Monitoring of Carbon Dioxide Capture with Sodium Hydroxide in a Customized 3D-Printed Reactor without Forced Mixing, Sustainability 14 (2022) 10795, https://doi.org/10.3390/su141710795.

[45] PubChem, (n.d.). https://pubchem.ncbi.nlm.nih.gov/compound/Carbon-dioxide (accessed April 28, 2023).

[46] SpectraBase, (n.d.).

[47] N.H. Do, H.H. Pham, T.M. Le, J. Lauwaert, L. Diels, A. Verberckmoes, N.H.N. Do, V. T. Tran, P.K. Le, The novel method to reduce the silica content in lignin recovered from black liquor originating from rice straw, Sci. Rep. 10 (2020) 21263, https://doi.org/10.1038/s41598-020-77867-5.

[48] S. Jose, L. Mishra, G. Basu, A. Kumarsamanta, Study on Reuse of Coconut Fiber Chemical Retting Bath. Part II—Recovery and Characterization of Lignin, J. Nat. Fibers (2017) 1–9, https://doi.org/10.1080/15440478.2016.1212772.

[49] M. Hartman, K. Svoboda, M. Pohořelý, M. Šyc, Thermal decomposition of sodium hydrogen carbonate and textural features of its calcines, Ind. Eng. Chem. Res 52 (2013) 10619–10626, https://doi.org/10.1021/ie400896c.